[12]M. Aegerter and F. Lüty, Bull. Am. Phys. Soc. 14, 872 (1969), and to be published.

[13]Excitation was maintained for as short a time as possible in order to minimize reorientation for 500-nm excitation or bleaching for infrared excitation.

[14]The efficiency is defined here for absorption by M^+ centers. This absorption decreases by about a factor of 2 in going from 100 to 150°K.

[15]H. Hirai, M. Ikezawa, and M. Ueta, J. Phys. Soc. Japan 17, 724 (1962).

[16]See, for example, I. Schneider, M. Marrone, and M. N. Kabler, to be published.

OBSERVATION OF ACOUSTICALLY INDUCED PHASE-MATCHED OPTICAL HARMONIC GENERATION IN GaAs

G. D. Boyd and F. R. Nash
Bell Telephone Laboratories, Holmdel, New Jersey 07733

and

D. F. Nelson
Bell Telephone Laboratories, Murray Hill, New Jersey 07974

(Received 8 April 1970)

Radiation near 5.3 μm arising from the collinear phase-matched mixing of a 10.6-μm Q-switched laser beam and a pulsed ultrasonic shear wave has been observed in GaAs. Phase matching occurs when the crystal momentum of the acoustic phonon is adjusted to equal the familiar momentum mismatch observed in conventional second-harmonic generation in cubic GaAs. Three components of the susceptibility governing the four-wave interaction process were measured.

For the first time the nonlinear phase-matched mixing between two infrared waves (angular frequency ω_F) and an acoustic wave (ω_A) to produce an output infrared wave (ω_C) has been observed.[1] Cubic GaAs was used. Since the acoustic frequency (15.7 MHz) was small compared with the optical frequency, the output frequency was extremely close to that of normal optical harmonic generation. The nonlinear four-wave interaction is weak and was observed only under conditions of phase matching. The interaction can be visualized physically as arising from a second-harmonic coefficient induced by the lattice distortion of the acoustic wave. Since the distortion and hence the coefficient will change sign every acoustic half-wavelength, phase matching will occur if the acoustic half-wavelength is made equal to the coherence length l_c of second-harmonic generation (SHG), that is,

$$\lambda_A/2 = l_c \equiv \pi/\Delta k, \tag{1}$$

where $\Delta k \equiv k_H - 2k_F$ and k_H is the wave vector of the second harmonic at $\omega_H = 2\omega_F$. Equation (1) yields the more familiar form of a phase-matching condition,

$$k_C = 2k_F + k_A, \tag{2}$$

since the output wave vector $k_C \cong k_H$. This possibility of using an acoustic phonon to achieve phase matching has also been considered by Harris, Wallace, and Quate.[2]

Two phase-matched interactions, forward-wave sum mixing (FWSM) and backward-wave difference mixing (BWDM), were observed. They are governed by

$$\omega_{C\pm} = 2\omega_F \pm \omega_{A\pm},$$
$$k_{C\pm} = 2k_F + k_{A\pm}. \tag{3}$$

The acoustic frequencies $\omega_{A\pm}$ needed for exact phase matching of the two interactions in these experiments differ only by 1.1 kHz. Since the full width at half-maximum of the phase-matching curve is 296 kHz for an interaction length of 1 cm, both FWSM and BWDM can be nearly phase matched simultaneously. In Fig. 1 are

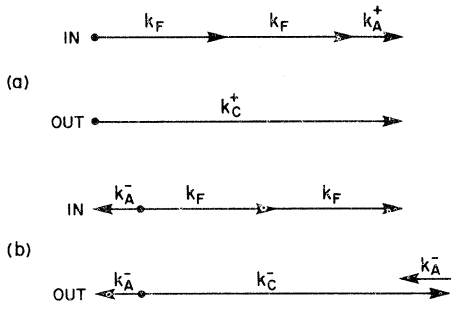

FIG. 1. Wave-vector conservation diagrams for (a) collinear forward-wave sum mixing and (b) backward-wave difference mixing.

shown the vector diagrams for wave-vector conservation for FWSM and BWDM. Note that for the case of BWDM an acoustic phonon is emitted, whereas for FWSM it is absorbed. FWSM and BWDM should be of equal strength under the conditions studied since the polarization generated is independent of the type of phase matching.

The nonlinear polarization at the combination frequency ω_C is proportional to the acoustic displacement gradient $u_{l,m}(\omega_A) \equiv \partial u_l/\partial x_m$ and to two electric fields at ω_F. In mks units we define the nonlinear coefficient f_{ijklm} by

$$\mathcal{P}_i(\omega_C) \equiv \epsilon_0 f^{\omega_C \omega_F \omega_F \omega_A}_{ijklm} E_j(\omega_F) E_k(\omega_F) u_{l,m}(\omega_A), \quad (4)$$

where $\mathcal{P}_i$, E_i, and $u_{i,j}$ represent peak Fourier amplitudes of the nonlinear polarization, electric field, and displacement gradient waves and repeated indices indicate summation. f_{ijklm} is nonzero only in noncentrosymmetric crystals and $f_{ijklm}u_{l,m}$ plays a role similar to the nonlinear coefficient d_{ijk} of SHG. The many sources of this nonlinearity and its symmetry will be discussed elsewhere.[3] Since the output power is proportional to the square of $\mathcal{P}$, it will be linear in acoustic power and quadratic in input optic power.

Since accurate absolute measurements of nonlinear coefficients are difficult in pulsed experiments, we chose to compare the strength of the acoustically induced harmonic with normal SHG. The power P_C radiated at ω_C was measured at phase matching and compared with the SHG power P_H radiated from a single-coherence-length crystal of GaAs with the same experimental arrangement. The SHG was observed in a collinear interaction in the [110] direction with E_F in the $[1\bar{1}1]$ direction. Absolute measurement of P_H yielded a value consistent with recent measurements[4-6] of the nonlinear coefficient, indicating that our apparatus was functioning properly. By assuming that the beam cross section at ω_F is the same in both cases and that the GaAs crystals of both experiments are in the near field of the focused fundamental beam[7] (i.e., short compared with the confocal parameter), the relative powers generated from the same fundamental laser beam can be shown to be

$$\frac{P_C}{P_H} = 2\,\frac{(f\nabla u)^2 l^2 \sin^2\varphi_A/\varphi_A{}^2}{\frac{4}{3}(d_{14} l_c 2/\pi)^2}, \quad (5)$$

where l is the length of the crystal over which the acoustic and optic fields interact. d_{14} is the coefficient of normal SHG, $\varphi_A \equiv \pi \Delta f_A l/v_A$, and Δf_A is the frequency departure from exact phase matching. At the latter condition $\sin^2\varphi_A/\varphi_A{}^2 = 1$. The full width of the phase-match curve at half-maximum can be calculated to be (0.296 MHz cm)/l using $v_A = 3.345 \times 10^5$ cm/sec characteristic of a shear wave traveling along [001] in GaAs.[8] The factor of 2 in Eq. (5) represents the sum of FWSM and BWDM powers for equal acoustic intensities for each interaction.

A number of components of f_{ijklm} are nonzero for the point-group symmetry of GaAs ($\bar{4}3m$). In this Letter we report the values of three components whose measurement was possible in a single transducer geometry corresponding to collinear propagation in the [001] direction. This orientation was chosen because normal SHG is forbidden by symmetry in this direction. The components measured and the field orientations used are

$$f_{11123}\text{: } E(\omega_F) \| [100] \| E(\omega_C);$$
$$f_{12223}\text{: } E(\omega_F) \| [010],\ E(\omega_C) \| [100];$$
$$f_{22123} = f_{21223}\text{: } E(\omega_F) \| [110],\ E(\omega_C) \| [010]. \quad (6)$$

In all cases an acoustic shear wave propagating in [001] with displacements in [010] was used.

The experiment used a 10.6-μm Q-switched CO_2 laser having a rotating 5-m mirror separated by 2.5 m from a flat dielectric output mirror. The beam was focused with a 10-cm focal length BaF_2 lens into a GaAs crystal along the [001] direction. The confocal parameter of the focused beam within the crystal was 2.6 cm and thus diffraction effects were negligible. The GaAs crystal used for most measurements was 1.6 cm long and was doped with chromium to yield a resistivity of 10^8 Ω cm. Crystals of other lengths (0.5 to 2.5 cm) and resistivities (down to 0.1 Ω cm) were also used with similar results. The laser power averaged 50 mW in the lowest order transverse Gaussian mode with a 0.2-μsec pulse length at a repetition rate of 400 sec^{-1} indicating a peak power of 625 W (higher powers often caused surface damage). The shear-wave transducer, made of PZT-5 ceramic, was 2.5 mm square with a 0.5-mm hole through which the fundamental beam entered the GaAs. The transducer impendance was low and stepped up to ~100 Ω through a 4/1 transformer. Acoustic powers up to 400 W were used. The acoustic pulse length was typically one round-trip transit time. The acoustic pulse was triggered by an anticipation pulse from the rotating mirror a few microseconds before the laser pulse to allow the acoustic pulse to fill the crystal. The timing of the laser pulse with respect to the acoustic pulse was variable. It was generally

set to coincide with the end of the acoustic pulse. The detector was a Ge:Au photoconductor operated at 77°K followed by wide-band amplifiers and a boxcar integrator.

The phase-matched interaction was clearly demonstrated by a variation of f_A as shown in Fig. 2. The experimental curve was centered at 15.7 MHz. This corresponds by Eq. (1) to a coherence length l_c of (107 ± 2) μm in good agreement with previous measurements.[4,6] The somewhat larger than ideal width of the phase-matching curve may be attributed to the effect of acoustic diffraction which fills in the region of the crystal not directly excited by the transducer. This leads to an effective interaction length (1.1 cm) less than the crystal length (1.6 cm) and hence to a broader phase-matching curve. Other experimental evidence that supports the interpretation as an acoustically induced harmonic is the linear dependence of P_C on P_A, the acoustic power, and the quadratic dependence of P_C on P_F, the fundamental power. We have also shown that the interaction strengths of the FWSM and BWDM are the same. The results[9] of our relative output power measurements are

$$|f_{11123}| = (0.9 \pm 0.5)d_{14},$$
$$|f_{12223}/f_{11123}| = 0.14,$$
$$|f_{21223}/f_{11123}| < 0.07, \quad (7)$$

with the major source of error arising from deduction of the displacement gradient in the crystal which was typically $u_{2,3} = 1.7 \times 10^{-4}$. We verified that the polarization of the output beam in the measurements of f_{11123} and f_{12223} was as expected by theory, that is, that f_{21123} and f_{22223} were not detectable. Note that for unity displacement gradient the measured interaction strength, $f_{11123}u_{2,3}$, would be comparable with the normal lower order SHG interaction strength.

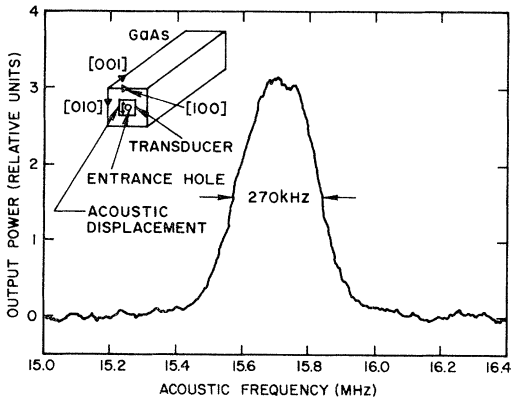

FIG. 2. Output power near 5.3-μm wavelength versus acoustic frequency. Inset shows crystal geometry.

The theory of this interaction[3] yields the following expressions for these coefficients:

$$f_{11123} = \chi_1^{\omega_C \omega_1 F \omega_2 F \omega_3 A},$$
$$f_{12223} = \chi_1^{\omega_C \omega_2 F \omega_2 F \omega_3 A} - 2d_1^{\omega_C \omega_2 F \omega_3 B} \chi_3^{\omega_B \omega_2 F \omega_3 A}/\kappa(\omega_B),$$
$$f_{21223} = \chi_2^{\omega_C \omega_1 F \omega_2 F \omega_3 A} - d_2^{\omega_C \omega_1 F \omega_3 B} \chi_3^{\omega_B \omega_2 F \omega_3 A}/\kappa(\omega_B) - d_3^{\omega_H \omega_1 F \omega_2 F} \chi_2^{\omega_C \omega_H \omega_2 A \omega_3}/\kappa(\omega_H). \quad (8)$$

The five-index susceptibility on the right represents the direct interaction of the two input optic waves and one input acoustic wave. The remaining terms represent indirect contributions to the susceptibility arising from acousto-optic scattering (frequency $\omega_B = \omega_F + \omega_A$) followed by optical mixing (frequency $\omega_C = \omega_B + \omega_F$) in two cases and from harmonic generation (frequency $\omega_H = 2\omega_F$) followed by acousto-optic scattering (frequency $\omega_C = \omega_H + \omega_A$) in the third case. In each of the indirect processes involved here the intermediate step corresponds to a longitudinal nonlinear polarization and hence does not correspond to any radiated field at either ω_B or ω_H. In Eq. (8) $d_{123} = d_{213} = d_{312} = d_{14}$ is the optical mixing coefficient (the factor of 2 arises from the mixing of two different frequencies); $\chi_{3223} = \chi_{2323} = \chi_{44} = -\kappa^2 p_{44}/2$ is one of the photoelastic susceptibility components (p_{44} is the Pockels photoelastic tensor component); $\kappa(\omega)$ is the dielectric constant.

Values for the direct-effect susceptibility components in Eq. (8) can be obtained from our measurements in conjunction with measurements of the other quantities in Eq. (8). Using a value[6] of $d_{14} = +1.3 \times 10^{-10}$ m/V with a plus sign,[4] $p_{44} = -0.068$[10] (extrapolated value for either 5.3 μm or 10.6 μm), $\kappa = 10.87$ at 5.3 μm,[11] and $\kappa = 10.69$ at 10.6 μm, we find $|\chi_{11123}| \approx 1.2 \times 10^{-10}$ m/V, $\chi_{12223} \approx (+0.8 \text{ or } +1.1) \times 10^{-10}$ m/V, and $+0.9 \times 10^{-10}$ m/V $\lesssim \chi_{21223} \lesssim +1.0 \times 10^{-10}$ m/V. The choice of values given for χ_{12223} arises because we measure only the absolute value of f_{12223}, while the range of values for χ_{21223} arises because we measure only an upper limit as well as an absolute value of f_{21223}. Note, however, that we have determined the absolute signs of two of the components based on our measurements and on the signs occurring in the indirect effects. Though the values of χ_{12223} and χ_{21223} we find are slightly different, we do not regard this as a violation of the Kleinman symmetry argument[12] by which they would be expected to be equal in the frequency range studied.

We wish to thank A. H. Meitzler for help and advice concerning the transducers, W. J. Nowotarski and S. Bortas for fabricating the transducers, and W. R. Wolff for technical assistance in the measurements. We also wish to acknowledge helpful suggestions by A. Ashkin, D. A. Kleinman, and M. Lax.

[1]D. F. Nelson, G. D. Boyd, and F. R. Nash, Bull. Am. Phys. Soc. 14, 853 (1969).

[2]S. E. Harris, R. W. Wallace, and C. F. Quate, IEEE J. Quantum Electron. 4, 354 (1968), and unpublished report.

[3]D. F. Nelson and M. Lax, to be published.

[4]J. J. Wynne and N. Bloembergen, Phys. Rev. 188, 1211 (1969).

[5]W. D. Johnston, Jr., and I. P. Kaminow, Phys. Rev. 188, 1209 (1969).

[6]J. H. McFee, G. D. Boyd, and P. H. Schmidt, to be published.

[7]G. D. Boyd and D. A. Kleinman, J. Appl. Phys. 39, 3597, (1968).

[8]T. B. Bateman, H. J. McSkimin, and J. M. Whelan, J. Appl. Phys. 30, 544 (1959); R. W. Dixon, J. Appl. Phys. 38, 5149 (1967), quotes $v_A = 3.32 \times 10^5$ cm/sec.

[9]The coefficient f_{21223} was unobservable and differs from the preliminary measurement (Ref. 1) because of birefringence in the output narrow-band filter which upset the necessary polarization selection on the output beam.

[10]A. Feldman and D. Horowitz, J. Appl. Phys. 39, 5597 (1968).

[11]K. G. Hambleton, C. Hilsum, and B. R. Holeman, Proc. Phys. Soc. (London) 77, 1147 (1961).

[12]D. A. Kleinman, Phys. Rev. 126, 1977 (1962).

NEGATIVE CRYSTAL-FIELD SPLITTING OF THE VALENCE BANDS IN $CdSnP_2$

J. L. Shay
Bell Telephone Laboratories, Holmdel, New Jersey 07733

and

E. Buehler and J. H. Wernick
Bell Telephone Laboratories, Murray Hill, New Jersey 07974

(Received 21 April 1970)

The polarization selection rules governing the band-edge electroreflectance and photoreflectance spectra of $CdSnP_2$ are opposite to those observed in wurtzite II-VI semiconductors and to theoretical predictions for similar chalcopyrite semiconductors. This result is explained by a new valence-band model with the essential feature that the sign of the crystal-field splitting is opposite to that observed in wurtzite II-VI semiconductors.

The II-IV-V_2 compounds are ternary semiconductors which normally crystallize in the chalcopyrite structure. They have physical properties similar to the familiar diamond, zinc blende, and wurtzite semiconductors by virtue of their tetrahedral coordination.[1,2] It is reasonable, therefore, to expect that the optical and electronic properties of the chalcopyrite crystals can be predicted by extrapolating from the well-understood binary semiconductors. Although this assumption has been invoked often in the interpretation of various experiments,[1-4] it has never been placed on a sound experimental basis.

It was the original purpose of this work to establish the viability of this assumption by measuring the electroreflectance and photoreflectance spectra of $CdSnP_2$, and interpreting these spectra in terms of a slightly perturbed zinc blende band structure. Instead, we have found that the polarization dependences of the electronic transitions from the valence-band maxima to the lowest conduction-band minimum are opposite to those which have been predicted theoretically[3,4] for similar chalcopyrite crystals. The polarization dependences which we observe in $CdSnP_2$ are opposite to those observed in wurtzite II-VI semiconductors. To explain our results we propose for $CdSnP_2$ an ordering of the valence bands in which the chalcopyrite perturbation produces a negative crystal-field splitting of the valence-band maxima. The triply degenerate Γ_{15} in zinc blende is split in $CdSnP_2$ such that the nondegenerate level Γ_4 lies above the doubly degenerate Γ_5, just opposite to the ordering observed in II-VI wurtzite semiconductors.[5] The doubly degenerate state Γ_5 is then split by spin-orbit coupling. We conclude that the chalcopyrite crystal potential has significant effects on the electronic structure.

In Fig. 1 we present the electrolyte electroreflectance[6] spectra near the fundamental edge of solution-grown[7-9] $CdSnP_2$ measured, respective-